

Atomic Layer Deposition of SiO₂-GeO₂ multilayers

Jordi Antoja-Lleonart,^{1, a)} Silang Zhou,¹ Kit de Hond,² Gertjan Koster,² Guus Rijnders,² and Beatriz Noheda^{3, b)}

¹⁾Zernike Institute for Advanced Materials, University of Groningen, 9747AG Groningen,

The Netherlands

²⁾MESA+ Institute for Nanotechnology, University of Twente, PO Box 217, 7522 NH Enschede,

The Netherlands

³⁾Zernike Institute for Advanced Materials, University of Groningen, 9747AG Groningen,

The Netherlands

(Dated: 7 April 2020)

Despite its interest for CMOS applications, Atomic Layer Deposition (ALD) of GeO₂ thin films, by itself or in combination with SiO₂, has not been widely investigated yet. Here we report the ALD growth of SiO₂/GeO₂ multilayers on Silicon substrates using a so far unreported Ge precursor. The characterization of multilayers with various periodicities reveals successful layer-by-layer growth with electron density contrast and absence of chemical intermixing, down to a periodicity of 2 atomic layers.

In the last four decades, Atomic Layer Deposition (ALD) has seen widespread adoption as a thin film growth technique^{1,2}. Its scalability, unprecedented conformality, and thickness control down to the atomic level, all make it a valuable asset to most nanofabrication efforts, playing a key role in commercial semiconductor manufacturing. Though chiefly known for the growth of relatively simple compounds, such as binary oxides, nitrides or sulfides, amorphous for the most part, ALD is also used to grow metals³, and recently more complex materials⁴, including perovskites⁵⁻⁹ have been realized as well.

One of the materials with the longest history using the ALD techniques is SiO₂¹⁰, a key element in the microelectronics industry with applications as passivation layer and gate oxide, among others. Less ubiquitous is the ALD growth of the related material GeO₂; its growth using ALD is relatively unexplored and not many of its possible precursors have been tested¹¹⁻¹³. Research on GeO₂ films has been mainly devoted to the study of the GeO₂/Ge interface, with GeO₂ films being proposed as a means to reduce the concentration of interface states between Ge and a high-K dielectric on top¹⁴⁻¹⁶, with the goal of realizing MOSFETs with a Ge-based channel. In these studies, thermal or plasma oxidation, as well as vapor growth^{17,18}, were used. It is worth mentioning that these works use precursors containing alkoxy or halide ligands, which give rise to comparatively slow reaction rates.

Thin films consisting of SiO₂ and GeO₂ multilayers have been investigated in the past, both from solution and vapor deposition methods¹⁹⁻²¹, with the focus being mostly on their optical properties. In this work, we show that using tetrakis(dimethylamino) germanium (IV) (TDMAGe) as precursor, it is possible to deposit GeO₂, as well as SiO₂/GeO₂ multilayers by thermal ALD.

We use a Picosun R-200 Advanced hot-wall ALD System whose chamber opens to a glovebox containing a nitrogen atmosphere, with controlled oxygen and water concentrations. We grow oxide thin films using

organometallic Si and Ge precursors. Respectively, these are bis(diethylamino) silane (BDEAS, commonly known as SAM-24) and tetrakis(dimethylamino) germanium (IV) (TDMAGe), both of them purchased from Air Liquide. The precursors are housed in canisters from Picosun, PicohotTM 300 and PicohotTM 200, which allow heating up to 260°C and 200°C, respectively. The organometallic precursors are delivered into the reaction chamber, through heated valve blocks, using nitrogen as carrier gas.

The oxidizer used in this work is ozone, which is produced from an INUSA Ozone Generator using Oxygen 6.0. Our valves allow a minimum opening time of 0.1s. Accessible process temperatures range from 100°C to 300°C, and the typical process pressure is 17 hPa. A temperature of 38°C for the BDEAS precursor bottle was established to give acceptable delivery rates. The TDMAGe bottle needed to be heated to 80°C to achieve similar precursor delivery rates to the reaction chamber. The gas lines downstreaming from the bottles were heated to 10-20°C above the temperature of their respective bottle to avoid precursor condensation taking place before reaching the reaction chamber.

The SiO₂ growth from BDEAS was optimized in collaboration with Picosun®. The reactor temperature was set to 300°C. The BDEAS pulse length was 0.1 s, followed by a 6.0 s N₂ purge. The ozone pulse length was 8.0 s, also followed by a 6.0 s N₂ purge. In our system, SiO₂ grown in this way shows a growth per cycle (GPC) of about 0.7Å. The GeO₂ growth has been independently optimized in the present work, as detailed below. The films are grown on 15x15 mm² square pieces of Si(100) wafers purchased from Microchemicals GmbH.

Thickness determination has been performed by ellipsometry using a J.A. Woollam Co. V-VASE system. In order to validate the ellipsometry results and to investigate the quality of the multilayers, X-ray reflectivity (XRR) has also been performed using a Bruker D8 Discover diffractometer with a high brilliance Cu rotating anode generator. The topographic features of the samples and their roughness were imaged by a Bruker Dimension Icon Atomic Force Microscope (AFM). Details on these methods are included in the Supplementary Material.

Although the growth of GeO₂ by ALD using TDMAGe as

^{a)}Electronic mail: j.antoja.leonart@rug.nl

^{b)}Electronic mail: b.noheda@rug.nl

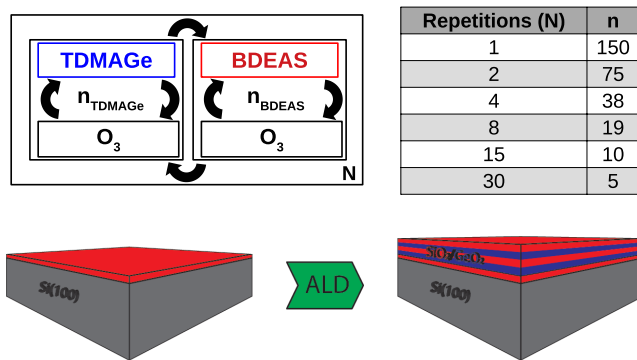


FIG. 1. Top left: Schematic representation of the synthesis method for the mixed oxide films. In our study, the pulse trains for the two precursors contain the same number of pulses: $n_{TDMAGe} = n_{BDEAS} = n$, and it varies from film to film. Top right: Table detailing the number of precursor pulses in each train (n) per sublayer and the total number of cycles (N) in the different films. For the 1:1 pulse ratio used in this work, the total number of cycles ($2n \times N$) was kept to approximately 300 for the whole series. Bottom: Sketch of the expected layered structure after growth.

a precursor was recently patented by ASM¹³, the details of the growth were not reported. Even though the precursors used for GeO_2 and SiO_2 are quite different, both of them use alkylamine ligands. This allowed us to optimize the GeO_2 growth, using as starting parameters those of the SiO_2 growth.

In the case of the combined SiO_2/GeO_2 multilayer growth, there are practical constraints to the process. First, the well-known SiO_2 precursor BDEAS^{22–27}, requires ozone or oxygen to function properly in thermal ALD. If water vapor is used instead, the Si-H bonds in the precursor do not react, which results in decreased growth rate and, possibly, leading to too high impurity concentrations in the film. For this reason, it is highly desirable to simplify the process by using ozone as the oxidizer in GeO_2 growth as well, even though this may lead to combustion-like reactions and less gentle oxidation. The ozone pulse length was fixed at 8s, sufficient to ensure a complete half-reaction.

Second, the SiO_2 growth is optimal at or above 300°C. When growing subsequent layers of different materials by ALD, it is in principle possible to change the reaction temperature when switching from one oxide to the next. However cooling and heating the reactor, even for relatively small temperature differences, are slow processes, making the growth time prohibitively long if the temperature needs to be changed repeatedly. For this reason, while the optimal growth temperature for pure GeO_2 is determined, if GeO_2 growth is still acceptable at 300°C, this temperature needs to be maintained in the multilayer growth.

Our system minimum operating temperature is, for this process, about 100°C. This is necessary to avoid condensation of the precursors or their reaction products in the chamber. Its maximum operating temperature is 300°C in its current configuration. Within this range, the growth rate of pure GeO_2 increases with increasing temperature, remaining approximately invariant above 150°C (Figure 2). One explanation for this

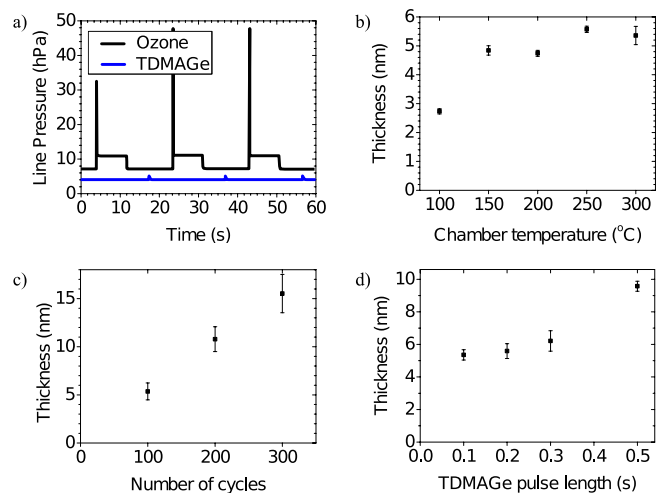


FIG. 2. a) Sketch of the pulse trains of the two precursors. b) GeO_2 film thickness after 100 cycles at various reactor temperatures. c) GeO_2 film thickness for different cycle numbers, at 300°C. A linear regression for this regime yields a GPC of 0.51Å. d) GeO_2 film thickness for 100 cycles and at 300°C for different TDMAGe pulse lengths. Error bars are estimates based on sample dispersion.

behaviour is that below 150°C the chemisorption reaction rate for TDMAGe is too low for proper ALD behavior, resulting in a decreased GPC. It could be argued that the stabilization of the GPC up to 300°C is an indication that precursor decomposition is still not significant at that temperature.

However, we can see that the GPC at 300°C increases for longer TDMAGe pulse lengths (Figure 2.d), while displaying approximately constant values for the short pulse lengths of 0.1s and 0.2s. This could indicate that this temperature is, in fact, sufficient to cause noticeable precursor decomposition, but that this has no noticeable effect in the growth provided that the TDMAGe pulses are short enough. This was confirmed by growing a film at 200°C using TDMAGe pulses of 0.5s. In that case the GPC was 0.53Å. This shows that the effect of precursor decomposition on thickness can be minimized either by growing at sufficiently low temperatures, which is difficult in our case, as discussed before, or by keeping the pulse length short. Therefore, the shortest pulse length of 0.1s was chosen. We further show that the thickness of the grown films follows a linear dependence with the number of pulses (Figure 2.c), as expected.

We then proceeded to grow multilayer heterostructures with alternating SiO_2 and GeO_2 sublayers. This layered growth is often characterized in the literature by the ratio between the number of pulses of the metal precursors of the two components. Here we have synthesized multilayers with different SiO_2/GeO_2 periodicities using a constant 1:1 pulse ratio and the same total number of pulses (same total thickness), but varying the number of pulses in each train. In this way, it is possible to control the degree of intermixing during the growth step, without resorting to post-annealing.

For the experiments here, we set the total number of cycles to 300, of which half will be GeO_2 and the other half SiO_2 .

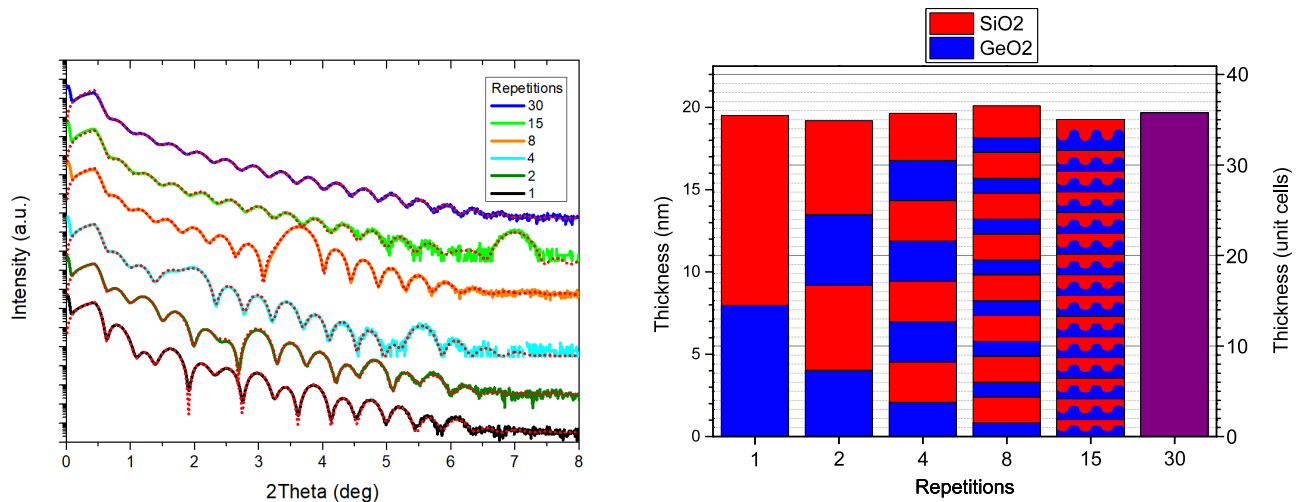


FIG. 3. Left: XRR scans and fits (red dashed lines) of the six films, from which the thicknesses were extracted. Right: Side view of the grown films, showing the actual layer thicknesses as determined by XRR. The red and blue stripes indicate layers made of different oxides, whereas the purple stripe is used for a layer of mixed oxide. Superlattice fits add the constraint that all SiO_2 layers and all GeO_2 layers in a single heterostructure have respectively the same thickness, but this constraint is relaxed for the top SiO_2 and the bottom GeO_2 layer in each case. The native SiO_2 layers, though both measured by ellipsometry prior to the ALD process and accounted for in the models, are not depicted here. Note that the models do include interface roughnesses. The right axis shows the thickness in multiples of 0.55nm , which is approximately the average between the SiO_2 and GeO_2 α -quartz form c -parameter, as it is used as a characteristic length scale of the material (though it is amorphous in this case).

Note that, assuming that the behaviour displayed in Figure 2 can be extrapolated to lower cycle numbers, the expected thickness for the GeO_2 and SiO_2 layers would be 8 nm and 11 nm , respectively, taking into account our previously mentioned GPC values at the optimized process parameters. Thus, assuming ALD linear regime, we expect a total thickness of 19 nm approximately, without accounting for the native oxide present on the wafer. This is in good agreement with the values obtained from the fitting of the XRR patterns, which give total thicknesses ranging between 19.2 nm and 20.1 nm (see Table 1 in Supplementary Materials).

The first experiment, with 150 cycles of TDMAGe/O_3 followed by 150 cycles of BDEAS/O_3 is denoted as "one repetition" (see Figure 1). One repetition, thus, contains a GeO_2 sublayer and a SiO_2 sublayer. In the following experiments, the number of cycles in each sublayer is subsequently halved, while the number of repetitions is doubled in order to keep the total number of pulses constant. The XRR patterns of these films, their fits and an illustration of the models used in the fits, are plotted in Figure 3 (the actual parameters of the model can be found in Table 1 of the Supplementary Material). By differentiating the experimental data (which has been obtained with a step size of 0.01° in 2θ) at low angles and smoothing it with a Savitzky-Golay filter, we determined the critical angle for all the films to be $0.235^\circ \pm 0.005^\circ$, independent of the number of repetitions (or the periodicity of the multilayer), close to the bulk value for SiO_2 (0.234° for a density of 2.65g/cm^3).

The XRR patterns show clear thickness oscillations in all cases, indicating the good homogeneity of the films and the quality of the top and bottom interfaces. In addition, the

patterns corresponding to the films containing from 2 up to 15 repetitions, all display superlattice reflections, attesting for the presence of chemical contrast between the SiO_2 and GeO_2 sublayers. The XRR pattern of the film with 15 repetitions shows its superlattice signature peak at about 7.1° , corresponding to a period of 12 \AA , which is approximately the size of two unit cells in SiO_2 and GeO_2 crystalline polymorphs. In the case of the 15 repetitions sample, despite the clear superlattice peak, the model is not able to provide a reliable value for the thickness of the individual SiO_2 or GeO_2 sublayers. This can be understood looking at the roughness values (see Table 1 in Supplementary Material), which are of the order of the estimated sublayer thickness (6 \AA). For the 30 repetitions film, only 5 pulses were provided, alternately, for each SiO_2 and GeO_2 sublayer, until completing the total of 300 pulses. Therefore, the superlattice periodicity is expected to be half of the value of the periodicity displayed by the 15 repetitions films, 6 \AA . This value is similar to the roughness values obtained with the reflectivity fit and, thus, no chemical contrast is expected. Indeed, in this case, the superlattice model also gives unreliable results but, unlike in the case of the 15 repetition film, the 30 repetition XRR pattern can be modelled by a uniform layer (see Table 1 in Supplementary Material), consistent with the absence of superlattice peaks up to an angle of 14° .

From this series of experiments it becomes clear that electron density, or composition, contrast between the SiO_2 and the GeO_2 sublayers is present down to the atomic level (close to a unit cell of their stable polymorphs). On the one hand, these results attest the excellent capabilities of ALD in general, allowing the growth of heterostructures with atomic-

scale thickness control. On the other hand, it nicely illustrates a potential pitfall of the layered approach to compositional tuning in ALD, in that extremely short supercycles are needed in order to achieve a uniform composition rather than a superlattice.

As a final note, it must be pointed out that, as directly visible in Figure 3, the $\text{SiO}_2:\text{GeO}_2$ thickness ratio, and therefore the atomic ratio, changes from one film to the next, even though the pulse ratio for all of them is maintained as a 1:1. This dependence of the composition on the precise pulsing sequence, and not only on the pulse ratio, has been previously observed²⁸.

To conclude, we have successfully optimized the ALD growth of GeO_2 thin films from TDMAGe and O_3 precursors. In order to successfully achieve $\text{SiO}_2/\text{GeO}_2$ films by sequential layered growth, a compromise has been found between the optimal growth parameters and those parameters that will allow us to synthesize a mixed oxide film in a reasonable amount of time. Armed with this knowledge, we have set out on the synthesis of a series of increasingly intermixed $\text{SiO}_2/\text{GeO}_2$ thin films, showing that ALD indeed is able to achieve atomic level accuracy for these compounds as well.

See the supplementary material for further details on the experimental methods, for the AFM images of the films, and for the details and fitting parameters giving rise to the XRR simulation curves in Figure 3.

The data that support the findings of this study are available from the corresponding author upon reasonable request.

I. ACKNOWLEDGEMENTS:

The authors are grateful to Picosun® for their optimization report related to the growth of SiO_2 , to Adrian Carretero-Genevri er and Vaclav Ocelık for useful discussions and to Ir. Jacob Baas and the Zernike NanoLab Groningen for the technical support. The authors also acknowledge financial support from NWO’s TOP-PUNT grant 718.016002.

REFERENCES:

- ¹R. L. Puurunen, “Surface chemistry of atomic layer deposition : a case study for the trimethylaluminum/water process,” *Journal of Applied Physics* **97**, 1–55 (2005), arXiv:Journal of Applied Physics vol. 97(2005):12, pp. 121301-121301-52.
- ²R. W. Johnson, A. Hultqvist, and S. F. Bent, “A brief review of atomic layer deposition: From fundamentals to applications,” *Materials Today* **17**, 236–246 (2014).
- ³J. Hamalainen, M. Ritala, and M. Leskela, “Atomic Layer Deposition of Noble Metals and Their Oxides,” *Chemistry of Materials* **26**, 786–801 (2014).
- ⁴M. Coll and M. Napari, “Atomic layer deposition of functional multicomponent oxides,” *APL Materials* **7**, 1–15 (2019).
- ⁵M. Tyunina, M. Plekh, J. Levoska, M. Vehkamaki, M. Hatanpaa, M. Ritala, and M. Leskela, “Dielectric properties of atomic layer deposited thin-film barium strontium titanate,” *Integrated Ferroelectrics: An International Journal* **102**, 29–36 (2008).
- ⁶N. M. Sbrockey, M. Luong, E. M. Gallo, J. D. Sloppy, G. Chen, C. R. Winkler, S. H. Johnson, M. L. Taheri, G. S. Tompa, and J. E. Spanier,

- “LaAlO₃/SrTiO₃ Epitaxial Heterostructures by Atomic Layer Deposition,” *Journal of Electronic Materials* **41**, 819–823 (2012).
- ⁷A. R. Akbashev, G. Chen, and J. E. Spanier, “A facile route for producing single-crystalline epitaxial perovskite oxide thin films,” *Nano Letters* **14**, 44–49 (2014).
 - ⁸M. D. McDaniel, T. Q. Ngo, S. Hu, A. Posadas, A. A. Demkov, and J. G. Ekerdt, “Atomic layer deposition of perovskite oxides and their epitaxial integration with Si, Ge, and other semiconductors,” *Applied Physics Reviews* **2**, 1–32 (2015).
 - ⁹E. L. Lin, A. B. Posadas, L. Zheng, J. Elliott Ortman, S. Abel, J. Fompeyrine, K. Lai, A. A. Demkov, and J. G. Ekerdt, “Atomic layer deposition of epitaxial ferroelectric barium titanate on Si(001) for electronic and photonic applications,” *Journal of Applied Physics* **126**, 1–9 (2019).
 - ¹⁰Note 1, Occasionally “pulsed metal organic chemical vapor deposition” is used instead of ALD, though in practice both methods are very similar.
 - ¹¹P. R. Chalker, P. a. Marshall, P. J. King, K. Dawson, S. Romani, P. a. Williams, J. Ridealgh, and M. J. Rosseinsky, “Atomic layer deposition of germanium-doped zinc oxide films with tuneable ultraviolet emission,” *Journal of Materials Chemistry* **22**, 12824–12829 (2012).
 - ¹²V. Adinolfi, L. Cheng, M. Laudato, R. C. Clarke, V. K. Narasimhan, S. Balatti, S. Hoang, and K. A. Littau, “Composition-Controlled Atomic Layer Deposition of Phase-Change Memories and Ovonic Threshold Switches with High Performance,” *ACS Nano* **13**, 10440–10447 (2019).
 - ¹³R. H. Matero, “Atomic Layer Deposition of GeO₂ (US Patent),” (2014), arXiv:arXiv:1208.5721.
 - ¹⁴T. Yoshida, K. Kato, S. Shibayama, M. Sakashita, N. Taoka, W. Takeuchi, O. Nakatsuka, and S. Zaima, “Interface properties of Al₂O₃/Ge structures with thin Ge oxide interfacial layer formed by pulsed metal organic chemical vapor deposition,” *Japanese Journal of Applied Physics* **53**, 1–6 (2014).
 - ¹⁵S. Shibayama, T. Yoshida, K. Kato, M. Sakashita, W. Takeuchi, N. Taoka, O. Nakatsuka, and S. Zaima, “Formation of chemically stable GeO₂ on the Ge surface with pulsed metal-organic chemical vapor deposition,” *Applied Physics Letters* **106**, 1–4 (2015).
 - ¹⁶M. Kanematsu, S. Shibayama, M. Sakashita, W. Takeuchi, O. Nakatsuka, and S. Zaima, “Effect of GeO₂ deposition temperature in atomic layer deposition on electrical properties of Ge gate stack,” *Japanese Journal of Applied Physics* **55** (2016).
 - ¹⁷H. Matsubara, T. Sasada, M. Takenaka, and S. Takagi, “Evidence of low interface trap density in GeO₂/Ge metal-oxide-semiconductor structures fabricated by thermal oxidation,” *Applied Physics Letters* **93**, 1–3 (2008).
 - ¹⁸J. Robertson and R. M. Wallace, “High-K materials and metal gates for CMOS applications,” *Materials Science & Engineering R* **88**, 1–41 (2015).
 - ¹⁹Q. Y. Zhang, K. Pita, C. K. F. Ho, N. Q. Ngo, L. P. Zuo, and S. Takahashi, “Low optical loss germanosilicate planar waveguides by low-pressure inductively coupled plasma-enhanced chemical vapor deposition,” *Chemical Physics Letters* **368**, 183–188 (2003).
 - ²⁰C. K. F. Ho, H. S. Djie, K. Pita, N. Q. Ngo, and C. H. Kam, “Sintering and Porosity Control of (x)GeO₂ : (1-x)SiO₂ Sol-Gel Derived Films for Optoelectronic Applications,” *Electrochemical and Solid-State Letters* **7**, F96–F98 (2004).
 - ²¹C. K. F. Ho, K. Pita, N. Q. Ngo, and C. H. Kam, “Optical functions of (x) GeO₂ : (1-x) SiO₂ films determined by multi-sample and multi-angle spectroscopic ellipsometry,” *Optics Express* **13**, 1049–1054 (2005).
 - ²²S.-j. Won, S. Suh, M. S. Huh, and H. J. Kim, “High-Quality Low-Temperature Silicon Oxide by Plasma-Enhanced Atomic Layer Deposition Using a Metal-Organic Silicon Precursor and Oxygen Radical,” *IEEE Electron Device Letters* **31**, 857–859 (2010).
 - ²³M. L. O’Neill, H. R. Bowen, A. Derecskei-Kovacs, K. S. Cuthill, B. Han, and M. Xiao, “Impact of Aminosilane Precursor Structure on Silicon Oxides by Atomic Layer Deposition,” *The Electrochemical Society Interface* **20**, 33–37 (2011).
 - ²⁴S. B. Baek, D. H. Kim, and Y. C. Kim, “Adsorption and surface reaction of bis-diethylaminosilane as a Si precursor on an OH-terminated Si (0 0 1) surface,” *Applied Surface Science* **258**, 6341–6344 (2012).
 - ²⁵A. Mallikarjunan, H. Chandra, M. Xiao, X. Lei, R. M. Pearlstein, H. R. Bowen, M. L. O’Neill, A. Derecskei-Kovacs, and B. Han, “Designing high performance precursors for atomic layer deposition of silicon oxide,” *Journal of Vacuum Science & Technology A: Vacuum, Surfaces, and Films* **33**, 01A137 (2015).

- ²⁶G. Fang, L. Xu, J. Ma, and A. Li, "Theoretical Understanding of the Reaction Mechanism of SiO₂ Atomic Layer Deposition," *Chemistry of Materials* **28**, 1247–1255 (2016).
- ²⁷M. C. Schwille, T. Schössler, F. Schön, M. Oettel, and J. W. Bartha, "Temperature dependence of the sticking coefficients of bis-diethyl aminosilane and trimethylaluminum in atomic layer deposition," *Journal of Vacuum Science & Technology A: Vacuum, Surfaces, and Films* **35**, 01B119 (2017).
- ²⁸V. Longo, N. Leick, F. Roozeboom, and W. M. M. Kessels, "Plasma-Assisted Atomic Layer Deposition of SrTiO₃: Stoichiometry and Crystallinity Studied by Spectroscopic Ellipsometry," *ECS Journal of Solid State Science and Technology* **2**, N15—N22 (2013).